8 Outdoor thermal comfort within different courtyard buildings

The previous chapter showed that courtyards may provide a lower PET (and thus a more comfortable microclimate) during a longer period than the other urban forms investigated during the hottest day of the Netherlands. This chapter is parallel to Chapter 5, where the effect(s) of different courtyard orientations on pedestrians' thermal comfort will be explored. Then, the most and least comfortable courtyards will be taken as reference models for further modifications. The modifications include using vegetation, water and a high albedo material on the roof and the pavement of the courtyards. The study is based on simulations again for the hottest day in a reference year in the Netherlands.

Heat in courtyards: A validated and calibrated parametric study of heat mitigation strategies for urban courtyards in the Netherlands[1]

Mohammad Taleghani *[1] , *Martin Tenpierik* [1], *Andy. van den Dobbelsteen* [1], *David J. Sailor* [2]

1 Faculty of Architecture and the Built Environment, Delft University of Technology, Delft, the Netherlands

2 Department of Mechanical and Materials Engineering, Portland State University, Portland, OR, USA

Abstract

Outdoor thermal comfort in urban spaces is an important contributor to pedestrians' health. A parametric study into different geometries and orientations of urban courtyard blocks in the Netherlands was therefore conducted for the hottest day in the Dutch reference year (19th June 2000 with the maximum 33°C air temperature). The study also considered the most severe climate scenario for the Netherlands for the year 2050. Three urban heat mitigation strategies that moderate the microclimate of the courtyards were investigated: changing the albedo of the facades of the urban blocks, including water ponds and including urban vegetation. The results showed that a north-south canyon orientation provides the shortest and the east-west direction the longest duration of direct sun at the centre of the courtyards. Moreover, increasing the albedo of the facades actually increased the mean radiant temperature in a closed urban layout such as a courtyard. In contrast, using a water pool and urban vegetation cooled the microclimates; providing further evidence of their promise as strategies for cooling cities. The results are validated through a field measurement and calibration.

Key words

Urban courtyard blocks, climate change, urban microclimate, heat island mitigation strategies.

1 Published as: Taleghani M., Tenpierik M., Dobbelsteen A., Sailor, D., "Heat in Courtyards: A validated and calibrated parametric study of heat mitigation strategies for urban courtyards in the Netherlands", Solar Energy, 103(2014) 108-124.

§ 8.1 Introduction

Growing urbanisation and the extensive consumption of fossil fuels have a profound impact on the thermal environment in cities. The relatively low reflectivity of urban surfaces combined with high density of construction in cities results in an accumulation of heat in the urban environment. The general lack of green (vegetated) areas and surface water also makes cities warmer. As a result, the cooling demand of urban residents increases [1, 2] and the heat stress on pedestrians rises [3, 4]. Promising mitigation strategies have been developed in order to cool urban spaces. These strategies are mainly related to the configuration of the built environment in accordance with (un)favourable solar radiation, construction materials used, and presence of water and urban vegetation [5-9].

The novelty of this chapter is its focus on heat mitigation strategies in urban courtyard blocks in the Netherlands as one of the countries prone to climate change, i.e. becoming warmer and wetter [10, 11]. Thermal studies of urban courtyard designs are mainly studied in hot and arid environments and less in moderate Western Europe while there are several examples of the presence of this urban form in different Dutch cities (Figure 1). This chapter begins with a comprehensive review of strategies for cooling a microclimate. It then explores the application of these strategies to urban courtyards in the Netherlands. Courtyard blocks or building clusters are commonly used urban patterns in the Netherlands. In phase 1, the impact of different courtyard geometries and orientations are analysed; in the next phases, the courtyard models are studied in the context of the Dutch climate in 2050. Finally, three heat mitigation strategies are studied parametrically for the current situation on the following features: changing the albedo of the facades of the urban blocks, adding urban green, and adding water ponds.

Figure 1
Urban courtyard blocks in Amsterdam, Rotterdam and The Hague (left to right).

§ 8.2 Background

The following brief literature review considers studies of a) urban geometry and courtyards, b) microclimate design to cope with climate change, c) the effects of albedo on a microclimate, d) the effects of water on a microclimate, and e) the effects of vegetation on a microclimate.

A Urban geometry and courtyards

The interactions between urban geometry and surface properties under a specific climate generate microclimates. These interactions were first discussed by Olgyay [12] and Oke [3]. Givoni [13] discussed the thermal impact of urban typologies in different climates and arrived at general design guidelines. He writes that architectural forms, surface materials and urban morphology (compactness, elongations, etc.) can affect the microclimate environment. On this topic, courtyard blocks were studied in several climates addressing different benefits. A comprehensive study on urban courtyards at a latitude of 26-34°N was done by Yezioro, Capeluto and Shaviv [14] using the SHADING program. They showed that, for cooling purposes, the best direction of a rectangular courtyard was North-South (NS, i.e. with the longer facades on East and West), followed by NW-SE, NE-SW, EW (in this order). They found that the NS direction had the shortest duration of direct sun light in the centre of the courtyard. This finding is in accordance with climates (or seasons) in which less sun is desirable. They also investigated summer thermal comfort, and showed that, although the air temperature difference between shaded and unshaded areas was only 0.5 K, the mean radiant temperature was different up to 30 C [15]. Steemers, Baker, Crowther, Dubiel, Nikolopoulou and Ratti [16] proposed six archetypical generic urban forms for London and compared the incident solar radiation, built potential and daylight admission. They concluded that large courtyards are environmentally adequate in cold climates, where under certain geometrical conditions they can act as sun concentrators and retain their sheltering effect against cold winds. Herrmann and Matzarakis [17] simulated urban courtyards with different orientations in Freiburg, Germany. They showed that the mean radiant temperature (T_{mrt}) was highest for NS and lowest for the EW orientation at midday and at night. During the night, the mean radiant temperatures were very similar, but the orientation of the courtyard affects the time of the first increase of T_{mrt} in the morning, due to direct sun. In the Netherlands (on average at 52°N), few studies have addressed the Physiological Equivalent Temperature (PET) or other outdoor thermal comfort indices. Among these, van Esch, Looman and de Bruin-Hordijk [18] compared urban canyons with street widths of 10, 15, 20 and 25 meters, and EW and NS directions. They concluded that the EW canyons did not receive sun on the 21st of December, while during summer and in the morning and afternoon, canyons had direct sun; at noon the sun was blocked. On the shortest day, the NS canyons got some sun

for a short period (even the narrowest canyon) and were fully exposed to the sun in the mornings and afternoons.

B Microclimate design to cope with climate change

Global warming is likely to have a significant effect on cooling and heating loads in buildings. IPCC [19] provides (and updates) estimations for future climates through different climate scenarios. Accordingly, building and urban designers try to reduce cooling loads of buildings to cope with climate change in the future. The strategies that they use are mainly through:

- reducing solar heat loads, for instance with appropriate design, sun shading and reflecting materials [20-22];
- using natural cooling (provided by greenery, water and natural ventilation at night) [23, 24]; and
- using thermal mass in order to stabilise indoor temperatures [25, 26].

Vegetation can simultaneously block and reflect the sun and cool the environment through evapotranspiration. However, there are few studies addressing the effects of greenery in the context of future climate scenarios in the Netherlands. Outdoor thermal comfort needs to be studied to clarify how increasing urban greenery can provide a more comfortable environment in a warmer future.

C The effects of albedo on the microclimate

The albedo of a surface or material is defined as the fraction of incident solar radiation that is reflected [27]. High albedo materials therefore lead to lower surface temperatures, and a cooler ambient temperature through the mechanism of convection [28]. However, conventional materials used in urban environments such as asphalt, brick and stone pavements generally have low albedos (0.05, 0.2 and 0.4 respectively) [29, 30]. The use of these materials intensifies the urban heat island phenomenon. Several studies have reported that use of materials with low albedo and high specific heat capacity usually causes a larger temperature difference between the city and the countryside at night than during the day [31, 32].

In this regard, Doulos, Santamouris and Livada [33] compared 93 commonly used materials for outdoor pavements. They found that albedo depends on the visible colour, surface texture (roughness) and the type of material of a pavement. They concluded that smooth, flat and light tiles made of marble, mosaic and stone had higher albedo than concrete and granite. Conversely, although a higher albedo results in a lower surface temperature and consequently cooler indoor environment, it could

have negative consequences on the physical and mental health of pedestrians [34-36]. In the subtropical climate of Shanghai Yang et al. [37] showed that by increasing the ground surface albedo by 0.4, overall outdoor thermal comfort decreased as reflected by an increase in physiological equivalent temperature (PET) by 5–7°C. In this way, in a dense urban area with a hot climate, the albedo of vertical surfaces such as facades will play an important role for the pedestrian's thermal (and visual) comfort. In an extreme situation in Tokyo, the use of high albedo materials on the exterior opposite walls led to a higher indoor cooling demand because of the increased solar radiation reflected indoors through the windows [38]. Taleghani et al. [39] showed in the temperate climate of Portland (OR, USA) in a measurement showed a white material (with albedo 0.91) increased the globe and mean radiant temperature (0.9°C and 2.9°C respectively) while producing a cooler local air temperature (1.3°C) in comparison with a black pavement (with albedo 0.37). To sum up, the effect of albedo on both the indoor and the outdoor thermal environment can only be determined when studied in more detail for each urban situation.

D The effects of water on the microclimate

The cooling effect of ponds and canals on microclimates has been demonstrated in multiple studies [40, 41]. In the hot and dry climate of Bornos (Spain), for example, Reynolds and Carrasco [42] found summer temperature variations inside a courtyard with an enclosed pond from 26 to 29.5°C while the ambient temperature outside the courtyard varied between 22 and 44°C. Nakayama and Fujita [43] developed a water-holding pavement (consisting of porous asphalt and a water-holding filler) to increase water presence in urban spaces of Japan. They reported that the air temperature (T_a) above the water-holding pavement (when saturated) was 1-2°C lower than above the lawn and 3-5°C lower than above conventional pavements. In the hot and arid climate of Bahrain Radhi, Fikry and Sharples [44] showed that lack of water in an urban space could cause a 2-3°C temperature increase in the city and a 3-5°C temperature increase on artificial islands. In addition, through an optimisation study for the thermal comfort of an urban square in France, Robitu et al. [45] reported that the presence of trees and water ponds reduced the mean radiant temperature by 35-40°C at 1.5 m above the ground.

E The effects of vegetation on the microclimate

Vegetation has been studied in urban climates [46], mostly in regard to the urban heat island effect (first studied by Luke Howard in the early 19th century [47]). In contrast to the urban heat island, the park cool island can reduce the air temperature up to 3-4°C in summer [46, 48-50]. Vegetation cools the environment through two mechanisms [51]:

1 With a higher albedo compared to common pavements as asphalt and brick. Vegetation reflects more solar radiation [52]; moreover, with a lower specific heat capacity, green areas accumulate less heat [49, 53].

2 By evapotranspiration, which is the sum of evaporation (from the earth's surface) and transpiration (from vegetation). The ambient air is cooled by this phenomenon [3, 54, 55].

The evapotranspiration process requires a significant amount of energy from the microclimate. As noted by Montgomery [56] the latent heat of vaporisation of water is 2324 kJ/kg. Moffat and Schiller [57] found that latent heat transfer from wet grass can result in an air temperature 6–8°C cooler compared to a similar area with exposed soil. They also found that 1 m^2 of grass absorbs 12 MJ of heat on a sunny day.

The other advantage of green areas is their effect on the energy use for maintaining comfortable indoor environments. According to Akbari et al. [58], Wong et al.[59] and Carter and Keeler [60] trees and shrubs planted next to a building can reduce air conditioning costs by 15-35 % (and by 10 % of annual cooling demand). Likewise, the exposed surface of a black roof with a very low albedo can be as much as 50°C hotter than the roof surface under a vegetated green roof in summer [61].

While trees have the advantage to block the sun reaching the ground surface cooling the entire air space under their canopy, grass reduces the temperature mainly near ground level [62, 63]. Air temperature reductions due to vegetation are reported as: Miami 16°C, Tokyo 20°C, Singapore 5°C and Athens 8°C [64-67]. The potential cooling benefits of vegetation are increasingly being exploited in rooftop applications. Vegetated or "green" roofs have multiple benefits for the urban environment, including a reduction in storm water runoff, cooling of the urban climate system, and reduction in summer time heat transfer into buildings [6, 68, 69].

§ 8.3 Methodology

The study presented in this chapter consisted of five phases. In the first phase, 18 courtyard models were simulated using the ENVI-met software package for 19th June 2000, the hottest reference day in the Netherlands. These courtyards are given four directions: E-W, N-S, NE-SW and, NW-SE (see Figure 2, respectively row a, b, c and d). The dimensions of the courtyards inside the urban blocks vary between 10*10 m^2 and 10*50 m^2 with steps of 10 m.

ENVI-met is also needed to be validated and calibrated for the climate of the Netherlands. This process is extensively explained in Section 3.3.

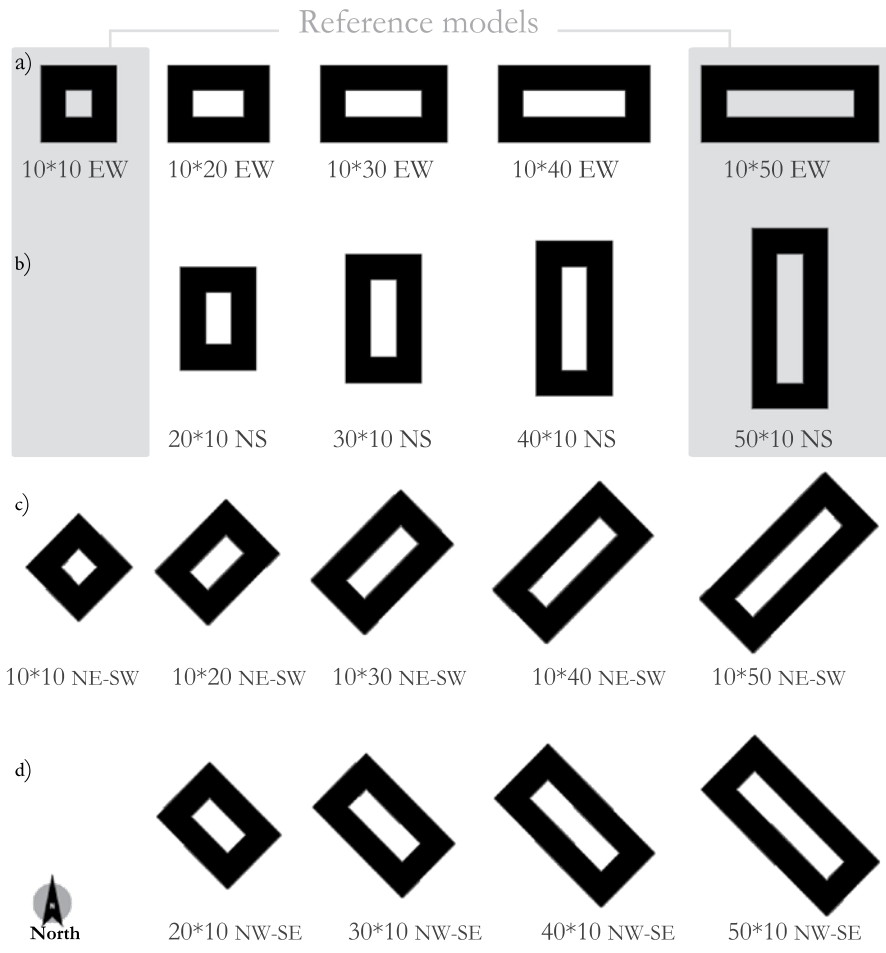

Figure 2
Overview of the basic models for the parametric study, E-W (1st row), N-S (2nd row), SW-NE (3rd row) and NW-SE (4th row). The reference models used in phases 2 to 5 are highlighted in grey. The dimensions are for the size of the courtyards, and the buildings have a depth of 9 m.

In Phase 2, the effect of climate change in 2050 was studied. Three models from the previous phase, 10*10 m^2, 10*50 m^2 E-W (from row a in Figure 2), and 50*10 m^2 N-S (from row b), were selected as reference models. The other models in-between the

mentioned ones were not simulated, because the first phase showed that the thermal behaviour of these intermediate models follows a regular pattern, and the three selected are the extreme models (in size and thermal impact). The weather data used for the simulation of 2050 is explained in section 3.2.

In the 3rd phase, the effect of changing the albedo of the facades of the urban blocks was studied, again considering the three reference models. Specifically, the brick surfaces of the original model (with an albedo of 0.10) were replaced with white marble (0.55) and white plaster (0.93) [70] to check its effect on the microclimate.

In the 4th phase, the cooling effect of small bodies of water was tested through embedding a water pool inside the three reference models. The size of the pool was chosen such that in all models 65% of the ground is allocated to a water pool while the rest is still pavement.

In the 5th phase, the cooling effect of vegetation was addressed. The ground and the roof of the courtyard blocks were covered with grass.

In every phase of this study, the results of the reference models were compared with the results of phase 2 (Figure 3).

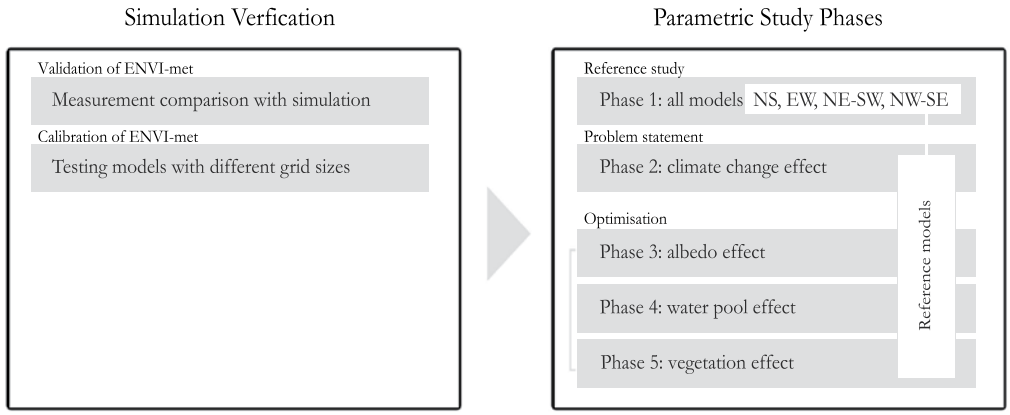

Figure 3
The research method of the chapter. First, the simulation software is validated through field measurement and calibration (left). Second, a comprehensive parametric study with simulation is done (right). In the first phase of the parametric study, 18 courtyard models are simulated in four directions. In the next phases, three reference models which are highlighted in Figure 2 are used for optimisation.

§ 8.3.1 Simulations

For the study discussed in this chapter, the hottest day of the Dutch reference year [71] was selected for the simulations (19 June 2000). This extreme day was selected to check the potential of the different courtyards in providing a comfortable microclimate in summer. All simulations were conducted using the urban computational fluid dynamics software ENVI-met 3.1 [72]. This program is a three-dimensional microclimate model designed to simulate the surface, plant and air interactions in an urban environment with a typical resolution of 0.5 to 10 meters in space and 10 second in time. ENVI-met can calculate the air temperature (°C), vapour pressure (hPa), relative humidity (%), wind velocity (m/s) and mean radiant temperature (°C) of the centre of models [73]. This program has been extensively validated and used widely for studying the effect of climate change [74, 75] and the impact of natural elements on a microclimate [73, 76, 77]. Table 1 shows the simulation conditions used for the first phase of this study.

Simulation day	19.06.2000
Simulation period	21 hours (04:00-01:00)
Spatial resolution	1m horizontally, 2m vertically
Initial air temperature	19°C
Wind speed	3.5 m/s
Wind direction (N=0, E=90)	187°
Relative humidity (in 2m)	59 %
Cloud coverage	0 Octa (clear sky)
Indoor temperature	20°C
Thermal conductance	0.31 W/(m²K) (walls), 0.33 W/(m²K) (roofs)
Albedo	0.10 (walls), 0.05 (roofs)

Table 1
The conditions used in the basic simulations (phase one of the parametric study).

§ 8.3.2 Climatic data

The climate of De Bilt (52°N, 4°E), is fairly typical of the Netherlands, and is classified as a temperate climate zone based on the climatic classification of Köppen-Geiger [78]. The wind is omnidirectional but South-West is prevailing. The mean annual dry bulb temperature is 10.5°C. For this chapter, the reference weather data of De Bilt was

used for the simulations and calculations according to Dutch NEN-5060 standard [71]. According to this standard, every month of the reference year is represented by a month from a specific year which is considered representative of the period from 1986 until 2005. The process for developing this reference year is very similar to the approach for developing Typical Meteorological Year data [79].

Regarding the future climate scenario in 2050, The Royal Dutch Meteorological Institute (KNMI) has translated the IPCC variants to four main scenarios in the near future in 2050, divided as in a matrix of two times two: a moderate and warm scenario (+1°C and +2°C temperature increase respectively) versus unchanged or changed air circulation patterns: G (moderate and unchanged air circulation), G+ (moderate and changed air circulation), W (warm and unchanged air circulation), W+ (warm and changed air circulation). Recent insights indicate a greater probability towards W and W+ rather than G and G+, implying higher temperatures throughout the year as well as dryer summers and wetter winters. Table 2 presents an overview of climate characteristics for each of the four climate scenarios.

2050		G	G+	W	W+
Global temperature rise		+1°C	+1°C	+2°C	+2°C
Change in air circulation patterns		No	Yes	No	Yes
Winter	Average temperature	+0.9°C	+1.1°C	+1.8°C	+2.3°C
	Coldest winter day per year	+1.0°C	+1.5°C	+2.1°C	+2.9°C
	Average precipitation amount	+4%	+7%	+7%	+14%
	Number of wet days (≥0.1 mm)	0%	+1%	0%	+2%
	10-day precipitation sum exceeded once in 10 years	+4%	+6%	+8%	+12%
	Maximum average daily wind speed per year	0%	+2%	-1%	+4%
Summer	Average temperature	+0.9°C	+1.4°C	+1.7°C	+2.8°C
	Warmest summer day per year	+1.0°C	+1.9°C	+2.1°C	+3.8°C
	Average precipitation amount	+3%	-10%	+6%	-19%
	Number of wet days (≥0.1 mm)	-2%	-10%	-3%	-19%
	Daily precipitation sum exceeded once in 10 years	+13%	+5%	+27%	+10%
	Potential evaporation	+3%	+8%	+7%	+15%
Sea level	Absolute increase	15-25 cm	15-25 cm	20-35 cm	20-35 cm

Table 2
Climate change scenarios for 2050 in the Netherlands [80].

In this chapter, the W+ scenario was selected as it is the most extreme scenario for 2050 in comparison with the current climate. Taleghani, Tenpierik and van den Dobbelsteen [81] explain how weather data for the year 2050 is constructed from these KNMI climate scenarios. In the weather file for the year 2050, solar radiation intensity has not changed since it mainly depends on latitude. However, cloud coverage and precipitation could not be changed as compared to the current climate because detailed data for the climate scenarios is lacking. The weather file for the year 2050 thus only differs from the weather file for the current climate concerning air temperature.

§ 8.3.3 Validation of ENVI-met

§ 8.3.3.1 Measurement versus simulation

In this research, one ENVI-met model was validated for the Netherlands through a comparison between field measurements and simulation results. The measurements were done within a courtyard building on the campus of Delft University of Technology. A wireless Vantage Pro2 weather station was used to measure among others drybulb air temperature with an interval of 5 minutes (Figure 4-a). The sensor of air temperature was protected by a white shield to minimise the effect of radiation. The height of the data logger is 2 m. The courtyard environment was measured for 16 days in September 2013. Two random days, September 22nd and 25th were selected for ENVI-met simulation. The weather data for the simulation were taken from a weather station located 300 meters from the courtyard. The data from simulations and measurements are compared in Figure 5 to show the accuracy of the simulation results. Moreover, the simulation input data are presented in Table 3.

The measured air temperatures between 21st and 26th of September are shown in Figure 5 with the black line. The two simulated days are drawn with the grey line (on 22nd and 25th). On the first day (22nd), the patterns of air temperature between measurement and simulation are more or less the same. On the second day (25th), the peaks of the hottest hour are different in number and in time. On the first day, the peak of T_a according to the simulation is 0.5°C higher than according to the measurement. On the second day, the peak of T_a according to the measurement is 1.2°C higher than according to the simulation. The root mean square deviation of the dry bulb temperature between simulation and measurement on the first day is 0.7°C and on the second day is 1.3°C. In Figure 5- right, the total data of simulation and

measurement in the two days are compared in one diagram. The correlation coefficient between the two sets of data is 0.80.

	First day	Second day
Simulation day	22.09.2013	25.09.2013
Simulation period	28 hours	28 hours
Spatial resolution	3m horizontally, 2m vertically	3m horizontally, 2m vertically
Initial air temperature	15.6°C	14°C
Wind speed	1.0 m/s	1.1 m/s
Wind direction (N=0, E=90)	245°	180°
Relative humidity (in 2m)	94 %	87 %
Indoor temperature	20°C	20°C
Thermal conductance	0.31 W/m²K (walls), 0.33 W/m²K (roofs)	0.31 W/m²K (walls), 0.33 W/m²K (roofs)
Albedo	0.10 (walls), 0.05 (roofs)	0.10 (walls), 0.05 (roofs)

Table 3
The conditions used in the validation simulations.

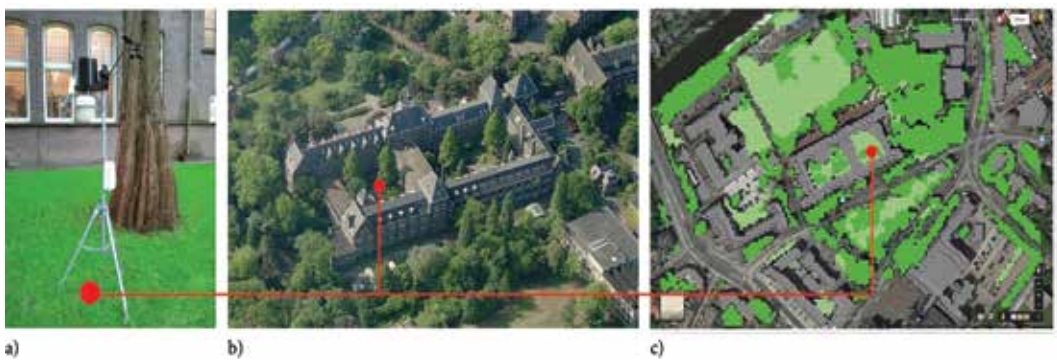

Figure 4
a) The weather station (Vantage Pro2) used for measurement in situ, b) the aerial photo of the measured courtyard, and c) the courtyard model and its surroundings in ENVI-met. The red line specifies the location of the weather station in the field and the receptor point in the computer model.

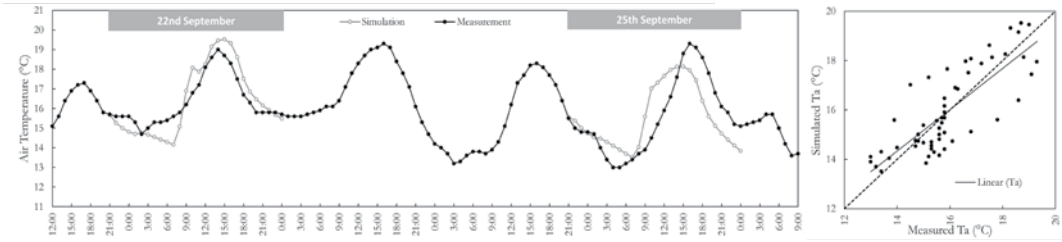

Figure 5

Comparison of the simulation results (on 22nd and 25th) with the measurements between 21st and 26th of September (left). The compared two day data are also illustrated in a scattered graph (right).

§ 8.3.3.2 Calibration of the ENVI-met simulations

To check the accuracy of the ENVI-met models, the reference models highlighted in Figure 2 are modelled with two different grid sizes (180*180 m^2 and 90*90 m^2). As it is shown in Figure 6-a, a courtyard model (10*50 m^2 EW) with 8 similar blocks in its surrounding is modelled in the 180*180 m^2 grid size. Then, the same courtyard model is simulated also in the 90*90 m^2 grid size withought neighbouring blocks (Figure 6-b). If the results of the reference models in the context of these two different grid sizes are identical, further simulations could be done with the smaller grid size (90*90 m^2) to reduce the simulation time.

For this calibration, the air temperature and mean radiant temperature within the courtyards are compared. The simulations are done under the conditions mentioned in Table 1. Figure 6-c shows the air temperature for the two grid sizes, and Figure 6-d shows both results as function of each other. Since the air temperatures in the two models do not exactly match, the trendline line in Figure 6-d is not perfectly 45°. This shows that there is a deviation between the two situations. In fact, the root mean square deviation of the two situations is 0.31°C. In Figure 6-e and 6-f, this comparison is done for the mean radiant temperature, and the root mean square deviation in this case is 0.74°C. This shows that mean radiant temperature is more deviated than air temperature between the two simulations.

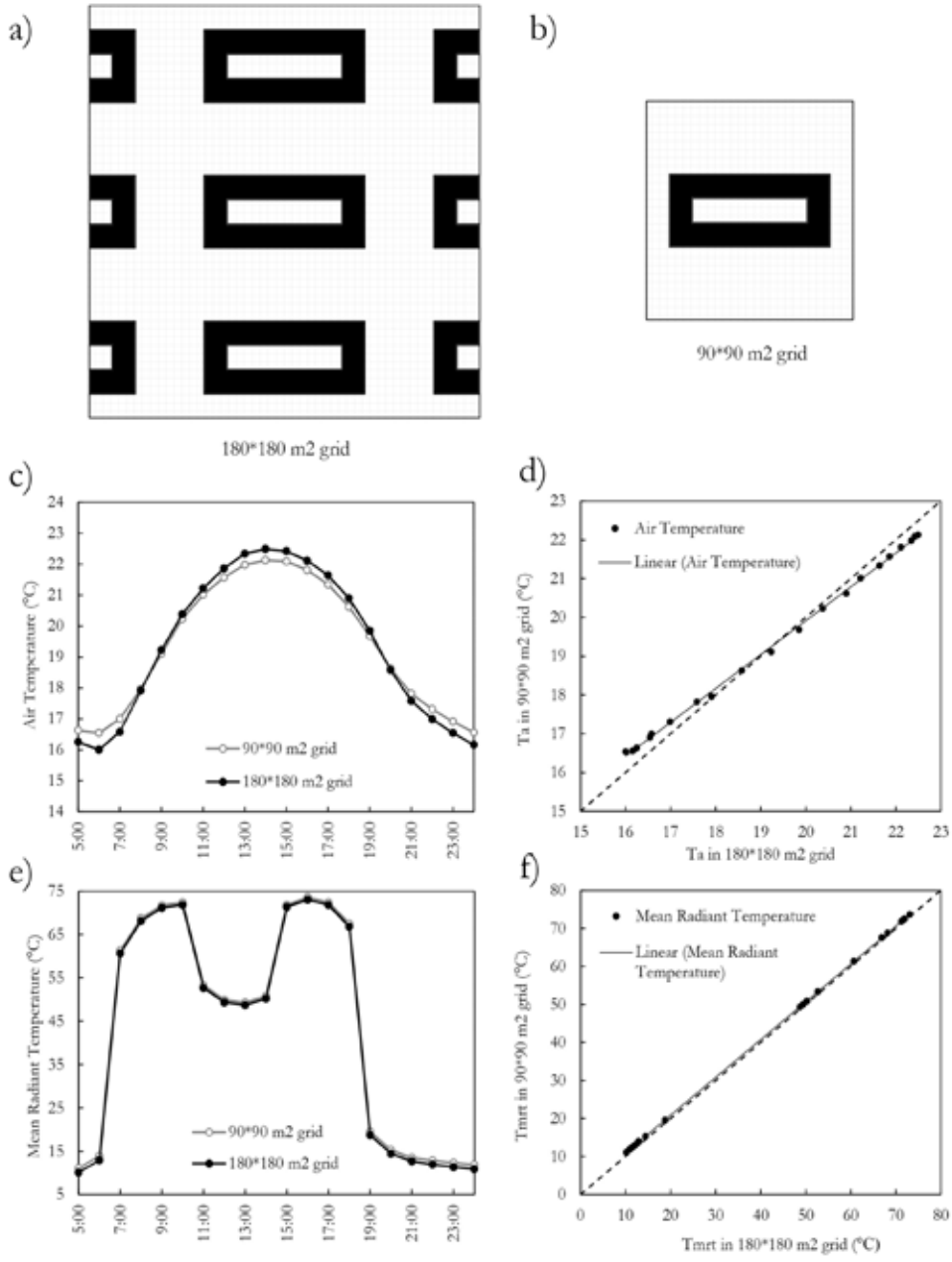

Figure 6

*a) the courtyard model 10*50 m² EW in 180*180 grid with similar neighbouring blocks, b) the same courtyard model withought neighbours and in 90*90 grid size, c) air temperature in different grid sizes, d) the comparison of the air temperatures in a scattered graph, e) mean radiant temperature in different grid sizes, and f) the comparison of the mean radiant temperatures in a scattered graph.*

This calibration procedure was repeated for the other reference models, 10*10 m^2 and 50*10 m^2 NS. The results are explained in Table 4. The average root mean square deviations for air temperature and mean radiant temperature in the reference models are 0.26°C and 0.98°C, respectively. This shows that further simulations with a 90*90 m^2 grid only, thus withought similar urban courtyard blocks, introduces a small but acceptable deviation in air and mean radiant temperature.

	RMSD* for T_a	RMSD for T_{mrt}
10*10 m^2	0.32	1.06
10*50 m^2 EW	0.31	0.74
50*10 m^2 NS	0.15	1.15
Average	0.26	0.98

Table 4
*The calibration data of models with two different grid sizes. *RMSD= root mean square deviation.*

§ 8.4 Results

§ 8.4.1 Phase 1: Reference study

In this step of the study, 18 urban blocks were simulated for 21 hours on the 29th of June 2000 (the hottest reference day in the Netherlands). The models vary in length and width from 10 to 50 m with steps of 10 m; and have four main orientations N-S, E-W, NW-SE, and NE-SW. The solar radiation reaching each courtyard was illustrated graphically, and also the mean radiant temperature of the receptor centred in each courtyard was described in this phase.

§ 8.4.1.1 Solar radiation

The first phase commenced with a solar radiation analysis for a point at the centre of each courtyard at 1.2 m height. On the summer day investigated, the sun rises at 05:18 h and sets at 22:03 h. Figure 7 illustrates the duration of direct solar radiation on the central point of each courtyard model. In the first row (a), the courtyards are directed

E-W. For this orientation, the duration of direct solar radiation increases from 4 hours and 32 minutes for the 10*10 m^2 courtyard to 11 hours and 44 minutes for the 10*50 m^2 E-W courtyard. Moreover, the first courtyard receives direct sun from 10:03 h till 14:35 h; the widest courtyard from 06:27 h till 18:11 h.

Regarding the second row (b), the courtyards are extended in N-S direction. In contrast to the previous urban blocks, the duration of direct solar radiation does not change if the size of the courtyard increases from 10*10 m^2 to 10*50 m^2; it is always 4 hours and 32 minutes. This shows that the east and west parts of the urban block are the main barriers against solar radiation.

In the third row (c), the urban blocks are rotated 45˚ towards NE-SW direction. Here, the courtyards are also extended from 10*10 m^2 to 10*50 m^2. The first rotated courtyard (10*10 m^2) receives direct sun at midday for 3 hours and 2 minutes. For the remainder of the models, this duration is 5 hours and 13 minutes starting at 10:48 h and ending at 16:01 h (mainly in the afternoon rather than in the morning).

In contrast, the last row (d) with NW-SE orientation has the same duration of direct solar radiation but between 08:37 h and 13:50 h. Insolation for this orientation happens mainly in the morning rather than in the afternoon. The duration of direct sun is described in Table 6 (Appendix).

Figure 7

The sun rays of the models on 19th of June. The grey regions show the period that direct sun light reaches the centre of the courtyards (between the first and last rays of sun). The Figure is produced by Sketchup (Chronoloux plugin). The data are taken at 1.60 meter height.

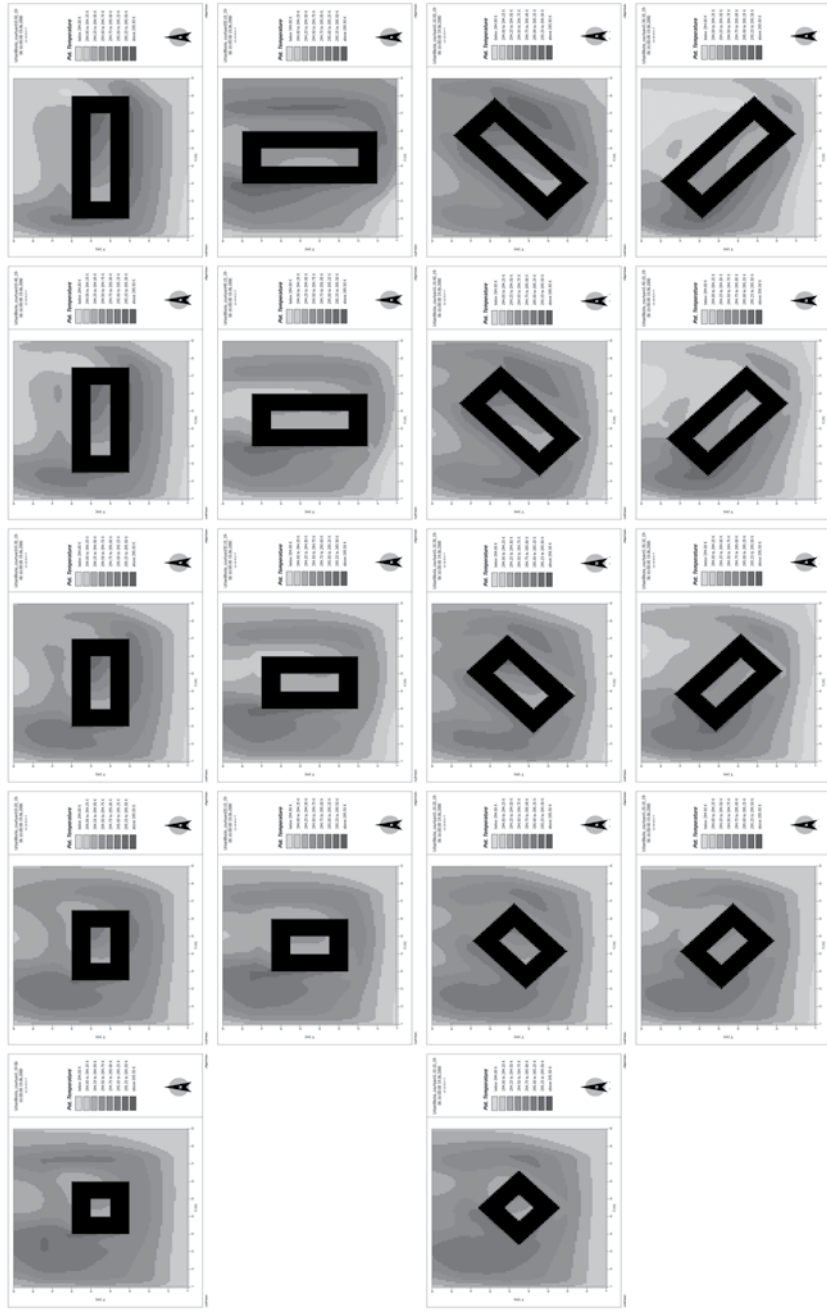

Figure 8
Air temperature distribution of the urban block models at 16:00 h (time of peak temperature), on the 19th of June. The data are taken at 1.60 meter height.

The mean radiant temperature, T_{mrt}, is defined as "*the uniform temperature of an imaginary enclosure in which the radiant heat transfer from the human body is equal to the radiant heat transfer in the actual non-uniform enclosure*" [82]. It is considered as a means of expressing the influence of radiation from surfaces and of solar radiation on human thermal comfort. In the outdoor environment, direct solar radiation plays the most important role. Figure 8 presents the mean radiant temperature of the central points inside the courtyards on the simulated day as calculated by ENVI-met.

In Figure 9a, corresponding to the urban blocks with E-W orientation (a), the mean radiant temperature suddenly rises when the sun irradiates the central point. In the 10*10 m^2 courtyard, this is exactly between 10:03 h and 14:35 h. This duration fits with Figure 7. This duration increases for the other models, all in correspondence to Figure 7. However, during midday a decrease in mean radiant temperature occurs for the last four models. During these hours the sun is very close to the southern façade of the courtyards.

In Figure 9b, corresponding to the urban blocks with N-S orientation (b), the times where T_{mrt} increases is in accordance with the times of direct solar irradiation. In this series of models, the duration of direct sun is the same for all models (4 h and 43 min). However, the differences between the 10*10 m^2 and the four other models is related to the southern part of the urban block. In the 10*10 m^2 model, the sunrays tip the top of the southern façade around noon as a result of which only scattered sunrays reach the centre point of the courtyard. However, by increasing the size of the courtyard to 20*10 m^2 N-S and beyond, the centre point gets full solar exposure around noon.To add up, T_{mrt} in these bigger urban blocks rises equally.

Considering Figures 8c and 8d, corresponding to the NE-SW and NW-SE orientations respectively (c and d), T_{mrt} rises and decreases in corresponce to direct solar exposure of the centre point. In this way, the first row of the rotated courtyards (NE-SW) receives direct sun mostly in the afternoon, and the fourth row of the courtyards (NW-SE) receives sun in the early morning. Consequently, T_{mrt} increases from noon till afternoon, and from early morning till early afternoon, respectively.

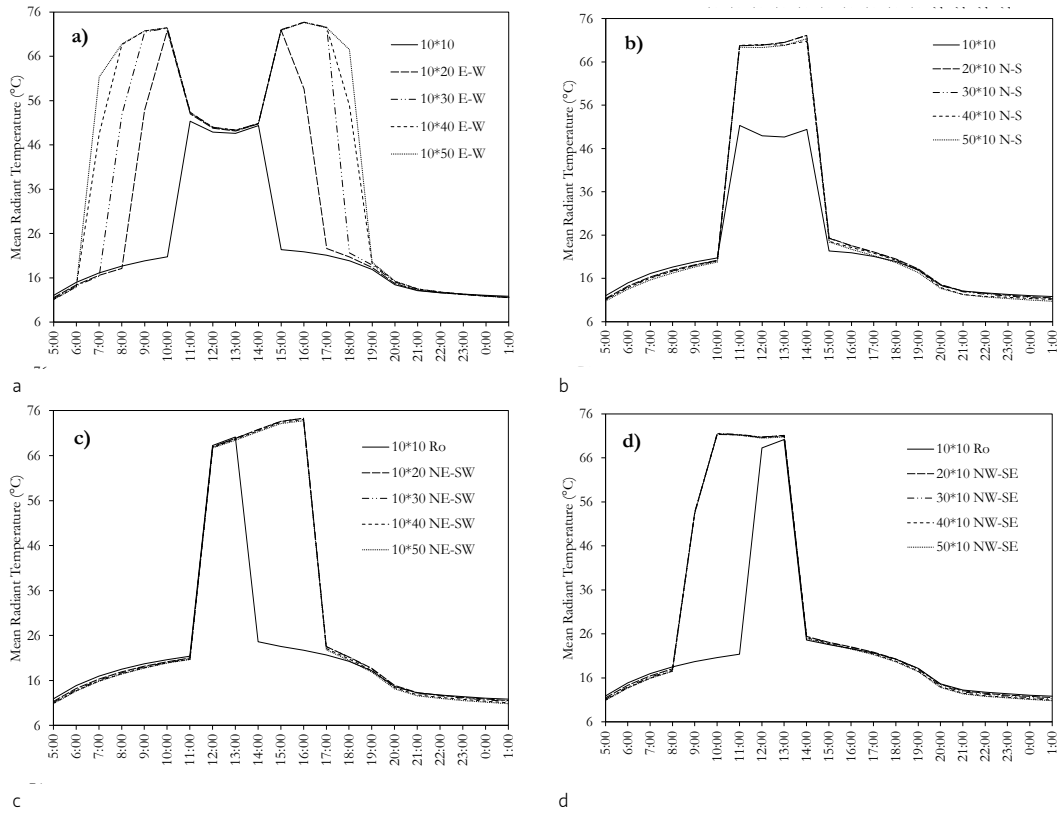

Figure 9

Mean radiant temperature at the height of 1.60 m at the centre of all urban blocks (a) to (d) with the same order as in Figure 7. Ro means that it corresponds to a rotated courtyard.

§ 8.4.2 Phase 2: the climate of 2050

In the second phase of this study, the three reference courtyard models were considered for the severest climate scenario for the Netherlands in 2050 (W+). As an illustration, two profile sections from the 10*50 m^2-EW model are shown in figure 10 in the current and future climate scenario. These sections are at 16:00 (the hottest hour in the reference year) and considering the orientation of the sun, the east parts of the courtyards are warmer than their west. In the current climate, the hottest temperature close to the ground is 23°C (296 K), while it is above 25°C in 2050.

Figure 11-a compares T_{mrt} of the reference models in 2050 (grey lines) to the current climate (black lines). As explained in the section on methodology, the weather data

for the year 2050 only differs from the weather data of the current climate in air temperature. Solar radiation duration and intensity are identical in both data sets. According to ISO7726 [82], Equation 1 shows how T_a has a small effect on T_{mrt}:

$$T_{mrt} = \left[(GT + 273.15)^4 + \frac{1.1*10^8*v_a^{0.6}}{\delta*D^{0.4}}(GT - T_a)\right]^{0.25} - 273.15 \quad (1)$$

Where T_{mrt} is the mean radiant temperature (K), GT is the globe temperature (K), v_a is the air velocity near the globe (m/s), δ is the emissivity of the globe which normally is assumed 0.95, D is the diameter of the globe (m) which typically is 0.15 m, and T_{a} is the air temperature (K).

Since the effect of T_a on T_{mrt} is very low, T_{mrt} is only slightly higher in 2050 than in the current climate. On the other hand, T_a increases by 3°C in the 2050 scenario. These results are more or less similar for all three reference models.

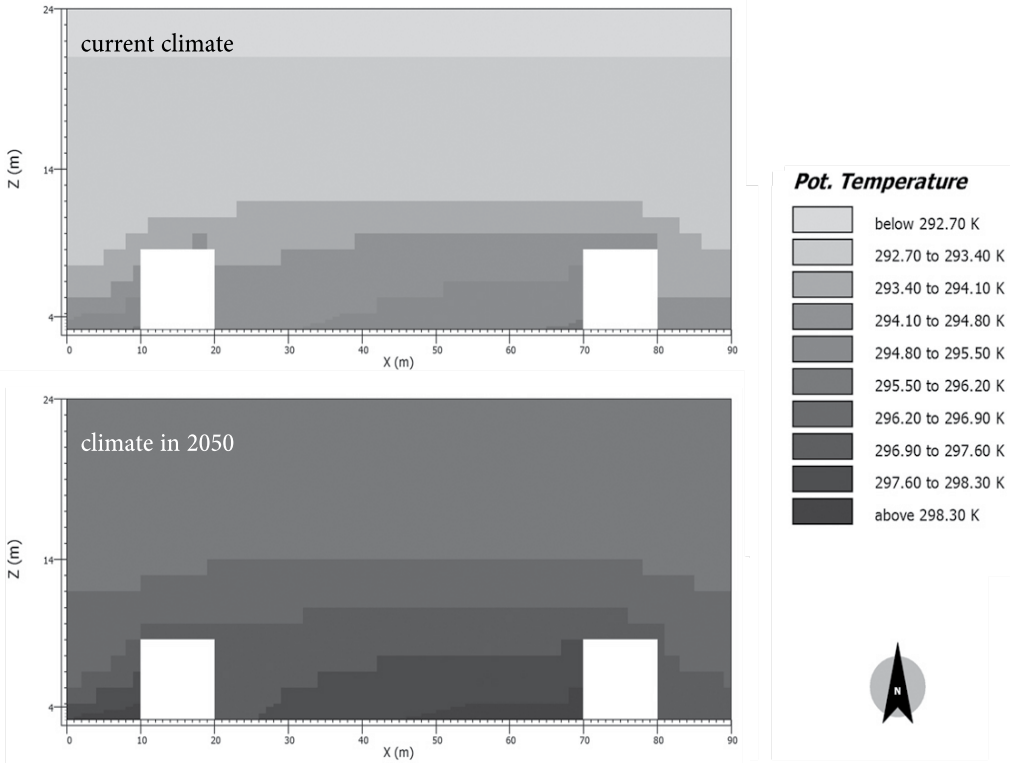

Figure 10
*Comparison of air temperature (potential temperature) of the 10*50 m² EW model in the current climate and in 2050 (on 19 June at 16:00).*

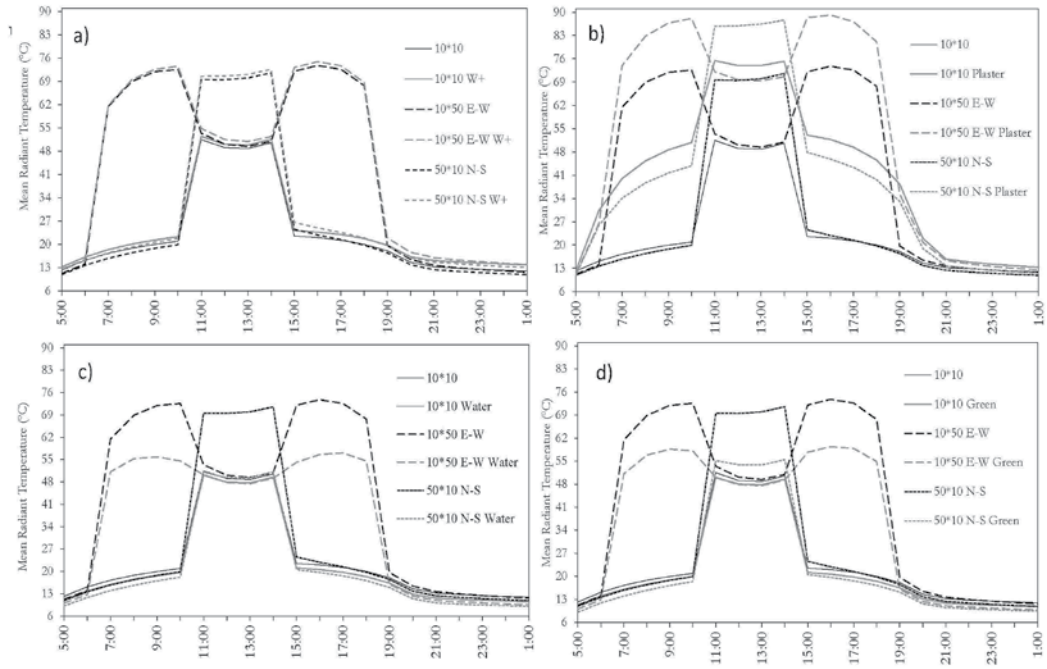

Figure 11
Mean radiant temperature of reference models in comparison with: a) the 2050 W+ climate scenario; b) higher albedo of plaster; c) courtyards with a water pool; d) courtyards with a green area.

Based on these differences between the current and the future climate in the Netherlands, the next three phases in the analysis investigated possible heat mitigation strategies.

§ 8.4.3 Phase 3: The albedo effect

In the third phase of this study, the albedo of the models' facades was increased. This change allowed us to understand whether higher albedo materials can help cool the microclimate of the courtyards or not. In the phase 1 and 2 simulations, the albedo of the facades was 0.10, representing dark brick. In the new simulations, the albedo was changed to 0.55 and 0.93, representing white marble and highly reflective plaster [70]. Light-coloured plaster, materials and paint are used in the countries close to the equator with a high solar radiation intensity. As a result, the increased albedo helps to reduce absorption of solar radiation. This phase of the study investigated the potential of this strategy for cooler climates.

Figure 12 shows how T_{mrt} change if a high albedo material replaces bricks on the facades of the urban blocks 10*50 m^2-EW. As can be seen, the model with plastered facades generally has a higher air temperature. The hotter air in this courtyard at 16:00 h located mostly at the eastern zone of the courtyard. Referring to Figure 13-b, the mean radiant temperature inside the courtyards with high albedo facades during solar exposure is higher than in the courtyards with low-albedo facades. Because of the higher albedo, more solar radiation is reflected towards the central receptor point. Since a courtyard is a closed urban form, there is a smaller probability to dissipate the solar reflections coming from buildings. In this way, the 10*10 m^2 courtyard has a higher increase (30 K at 15:00) in T_{mrt} than the bigger models. The maximum increase in the 10*50 m^2 EW model is +20°C (at 12:00), and +24°C (at 10:00) for the 50*10 m^2 NS model.

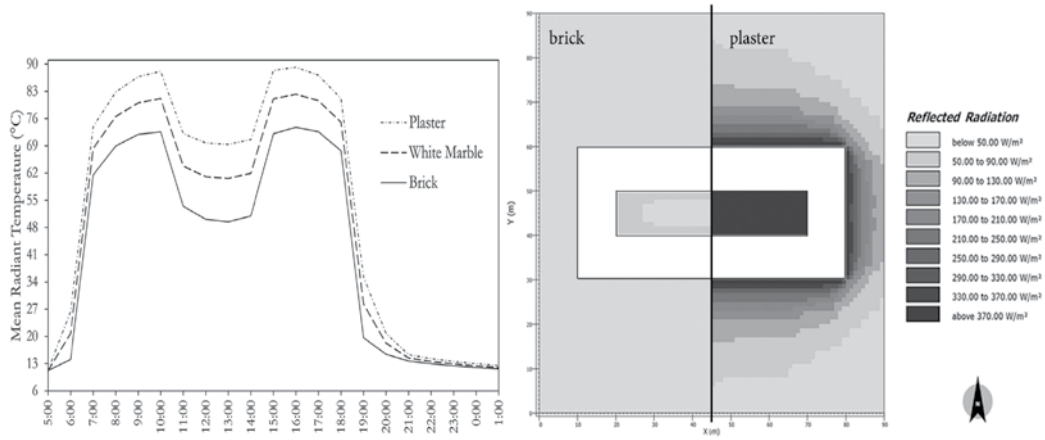

Figure 12

*The effect of increased surface albedo from brick (0.10) to white marble (0.55) and plaster (0.93) on mean radiant temperature of the 10*50 m^2 EW model (left) and reflected solar radiation (right).*

§ 8.4.4 Phase 4: The effect of water

Water installations such as fountains, canals, pools and ponds serve as heat buffers (with its high specific heat capacity as a thermal mass) at urban, neighbourhood and building scales. In the fourth phase of this study, the cooling effect of water (evaporation, heat buffering and thermal mass) was considered for the three reference models. A water pool was embedded on the ground inside the courtyard covering 65% of the area (the rest is left for walking (pavement)). Figure 13-c presents T_{mrt} of the models with water (grey lines) and compares this with the models without water from phase 1 (black lines).

The mean radiant temperature of the models with water is lower than of the models without water. For the 10*50 m^2-EW model, the maximum decrease is 18°C; and for the 50*10 m^2-NS model the maximum decrease is 21°C. Here it is worth mentioning that high-albedo materials (e.g. the plaster used in phase 3) and water are both highly reflective substances. The first showed a higher T_{mrt} in comparison with the phase 1 models while the latter showed lower T_{mrt}. In case of a water pond, water on the ground reflects the high-altitude summer sun back towards the sky and towards the receptor point. In contrast, the vertical high-albedo materials (plasters on the facades) reflect the sun towards the ground of the courtyard and also to the receptor point. Water has a high heat capacity as a result of which it does not heat up as quickly as the concrete pavement does. Additionally, the evaporation of water from the pond cools its surface and since the pond is close to the receptor point in the centre of the courtyard, it has a strong effect on T_{mrt}.

§ 8.4.5 Phase 5: The effect of vegetation

It was acknowledged in section 2 of this chapter that the greening of urban spaces and the installation of green roofs and porous pavements improves the air quality, reduces the ambient air temperature and consequently lowers indoor air conditioning energy demands. In the fifth phase of this study the ground of the courtyards and the roofs of the urban blocks were covered with grass.

The first benefit of the grass is that it blocks the sun to the ground level of the courtyards. Therefore, the soil absorbs less solar energy. Furthermore, the grass and soil cool the ground surface and air layer above by evapotranspiration, an effect similar to the evaporative cooling effect of the water ponds. In Figure 13-d, the differences between the green and reference microclimates are shown (respectively grey and black lines). The largest difference in mean radiant temperature is exhibited by the 50*10 m^2 NS courtyard with a 17°C cooler environment at 14:00 h due to the presence of grass.

§ 8.5 Discussion

Alteration of a building's geometry to receive or block sun is a common strategy in the early stages of climate-sensitive design. This strategy was explored in the first phase of this study. Different proportions of length to width in combination with four main orientations led to varied microclimates. The N-S courtyard direction has the shortest duration of solar radiation to penetrate into the courtyard, while the E-W orientation has the longest. The NW-SE orientation receives sun in the early morning while the NE-SW orientation mainly in the afternoon. Furthermore, by increasing the length of the courtyards only in the E-W direction, the duration of solar radiation can be increased. In this way, among the models the 10*50 m^2 EW courtyard model has the longest exposure to direct sun.

These results show that courtyards with N-S orientation are recommended for hot climates, and E-W oriented courtyards are more favourable for colder regions. In addition, the NW-SE direction is suitable when nights are cold and early morning sun is desired. In contrast, urban spaces in cold climates that are used for afternoon activities (like recreational squares) are more in accordance with NE-SW sun access.

Subsequently, the courtyard model with the longest duration of sun radiation (10*50 m^2 EW) was analysed and discussed to clarify the effects of different heat mitigation strategies: a) use of a higher albedo material, b) use of a water pool, and c) use of vegetation. These three strategies were analysed via their mean radiant temperature and air temperature.

As illustrated in Figure 12 (and Table 5), a high albedo of the facades leads to a higher mean radiant temperature (maximum +20°C increase at 12:00 h); a water pool inside the courtyard strongly reduces the mean radiant temperature (maximum -18°C at 15:00 h); vegetation also strongly reduces the mean radiant temperature (maximum -17°C at 15:00 h). Considering that the water pool covered 65% of the ground and the grass 100%, the cooling effect of water seems to be more effective. Here it is worthy mentioning that several studies have shown that increasing the albedo of facades leads to a cooler indoor environment; however; this chapter shows that outdoor environment performs different with higher albedos.

Figure 14 shows the air temperature of 10*50 m^2 EW courtyard model at 16:00 h, which was the hottest hour on the hottest reference day in the Netherlands. At this time, the sun irradiates the model from the south-west, and thus the north-east side inside of the courtyard is warmer, while the south-west side is cooler (Figure 14a). By increasing the albedo, the air temperature in the courtyard increases mainly in the eastern part (which is more irradiated than the western part at 16:00 h). Considering the outdoor space of the courtyard model (surrounding the building), the

air temperature in the regions outside the model (south and west) are more increased because of using higher reflectance materials on facades (Figure 14b). In the third situation adding a water pool decreases the air temperature inside the courtyard (Figure 14c); adding vegetation has a similar effect (Figure 14d). This is related to the effects of water and vegetation on T_{mrt}: water more strongly affects Tmr¬t than vegetation does. Furthermore, Figure 14 indicates the courtyard with water is cooler than the courtyard with green at 16:00. This is mainly due to the higher specific heat capacity of water. This allows water to absorb the sun during the day; in the afternoon, by releasing the heat, the courtyard will be warmer than the courtyard with green (which is partly shaded by grass and has absorbed less sun during the day).

	T_{mrt} (°C)	T_a (°C)	RH (%)
Ref study	42	19	72
High albedo	53	20	71
Water pool	35	19	75
Greened	36	19	77

Table 5
*The average mean radiant temperature (T_{mrt}), air temperature (T_a) and relative humidity (RH) of the 10*50 m² EW model.*

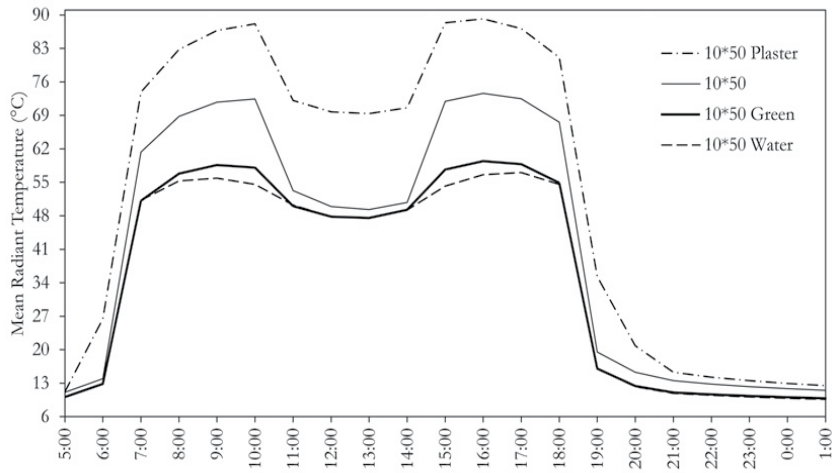

Figure 13
*Mean radiant temperature of the 10*50 m² EW courtyard model comparing different heat mitigation strategies.*

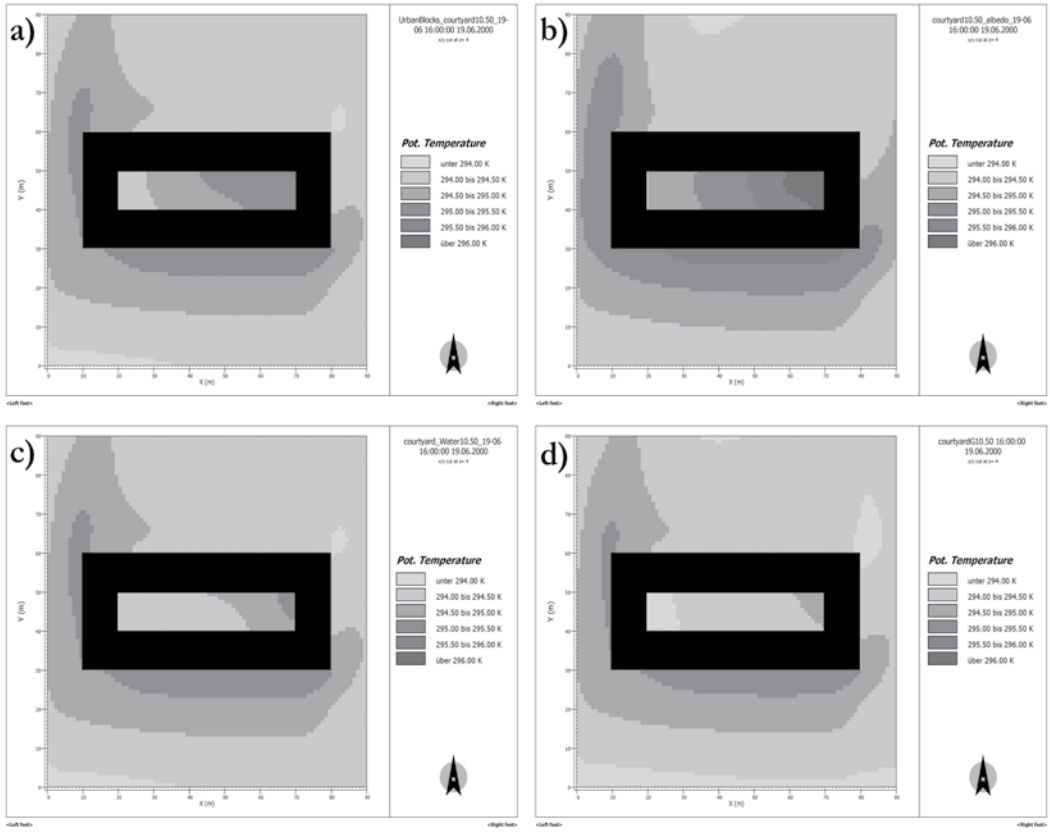

Figure 14

*Air temperature of the 10*50 m² EW courtyard model in different phases of the study: a) basic study, b) using high albedo facades, c) using water pool, and d) using grass.*

§ 8.6 Conclusions

The urban heat island phenomenon and climate change have led and will further lead to a temperature rise in urban spaces and cities. Therefore, there is a need for solutions to alter microclimates and provide a more desirable environment for pedestrians. This chapter investigated the outdoor microclimate of different urban blocks during the hottest reference day in the Netherlands. The courtyards were oriented in four main directions E-W, N-S, NE-SW and NW-SE. Subsequently, they were widened from a symmetrical 10*10 m² to 10*50 m² in E-W and other directions.

The first phase of the study showed that on a summer's day the E-W direction provides a long duration of direct sun. In contrast, the N-S direction provides the shortest period of sun radiation at the centre of a courtyard. Rotation of the models also showed that NW-SE-oriented courtyards receive sun in the early morning while NE-SW-oriented courtyards receive sun mostly in the afternoon.

Considering climate change and consequent global warming in 2050, three heat mitigation strategies were investigated. Increasing the albedo of facades led to an extensive increase of the mean radiant temperature (although it reduces indoor temperature). Using a water pool inside the courtyard or covering the ground of the courtyard with vegetation significantly reduced both the air temperature and mean radiant temperature. Finally, this research suggests using water pool and green areas are the most effective heat mitigation strategies for urban blocks in the Netherlands.

Appendix

a) E-W	10*10- 04h:32m	10*20- 07h:56m	10*30- 10h:00m	10*40- 11h:32m	10*50- 11h:44m
b) N-S		20*10- 04h:32m	30*10- 04h:32m	40*10- 04h:32m	50*10- 04h:32m
c) NE-SW	10*10- 03h:02m	10*20- 05h:13m	10*30- 05h:13m	10*40- 05h:13m	10*50- 05h:13h
d) NW-SE		20*10- 05h:13m	30*10- 05h:13m	40*10- 05h:13m	50*10- 05h:13m

Table 6
The duration of direct sun at the centre of the models in the reference study (Phase 1). h = hour, and m = minute.

References

1 H. Akbari, S. Konopacki, Energy effects of heat-island reduction strategies in Toronto, Canada, Energy, 29 (2004) 191-210.

2 M. Kolokotroni, X. Ren, M. Davies, A. Mavrogianni, London's urban heat island: Impact on current and future energy consumption in office buildings, Energy and Buildings, 47 (2012) 302-311.

3 T.R. Oke, Boundary Layer Climates, Routledge, New York, 1987.

4 K. Pantavou, G. Theoharatos, A. Mavrakis, M. Santamouris, Evaluating thermal comfort conditions and health responses during an extremely hot summer in Athens, Building and Environment, 46 (2011) 339-344.

5 H. Akbari, H.D. Matthews, Global cooling updates: Reflective roofs and pavements, Energy and Buildings, 55 (2012) 2-6.

6 S.S. Moody, D.J. Sailor, Development and application of a building energy performance metric for green roof systems, Energy and Buildings, 60 (2013) 262-269.

7 M. Santamouris, Cooling the cities – A review of reflective and green roof mitigation technologies to fight heat island and improve comfort in urban environments, Solar Energy, (2013).

8 M. Taleghani, M. Tenpierik, S. Kurvers, A. van den Dobbelsteen, A review into thermal comfort in buildings, Renewable and Sustainable Energy Reviews, 26 (2013) 201-215.
9 M. Taleghani, M. Tenpierik, A. van den Dobbelsteen, R. de Dear, Energy use impact of and thermal comfort in different urban block types in the Netherlands, Energy and Buildings, 67 (2013) 166-175.
10 IPCC, Climate Change 2007, in: S. Solomon, D. Qin, M. Manning, Z. Chen, M. Marquis, K.B. Averyt, M. Tignor, M. H.L. (Eds.) The physical science basis. Contribution of the working group I to the fourth assessment report of the intergovernmental panel on climate change, Cambridge, 2007.
11 KNMI, in: KNMI Klimaatscenarios. Transformatie tijdreeksen, KNMI, De Bilt, 2012.
12 V. Olgyay, Design with Climate, Princeton University Press, Princeton NJ, 1963.
13 B. Givoni, Climate Considerations in Building and Urban Design, Wiley, 1998.
14 A. Yezioro, I.G. Capeluto, E. Shaviv, Design guidelines for appropriate insolation of urban squares, Renewable Energy, 31 (2006) 1011-1023.
15 S. Berkovic, A. Yezioro, A. Bitan, Study of thermal comfort in courtyards in a hot arid climate, Solar Energy, 86 (2012) 1173-1186.
16 K. Steemers, N. Baker, D. Crowther, J. Dubiel, M.H. Nikolopoulou, C. Ratti, City texture and microclimate, Urban Design Studies, 3 (1997) 25-50.
17 J. Herrmann, A. Matzarakis, Mean radiant temperature in idealised urban canyons—examples from Freiburg, Germany, International Journal of Biometeorology, 56 (2012) 199-203.
18 M.M.E. van Esch, R.H.J. Looman, G.J. de Bruin-Hordijk, The effects of urban and building design parameters on solar access to the urban canyon and the potential for direct passive solar heating strategies, Energy and Buildings, 47 (2012) 189-200.
19 I.P.o.C. Change, Climate Change 2007 - The Physical Science Basis: Contribution of Working Group I to the Fourth Assessment Report of the IPCC, in, Cambridge, 2007.
20 M.J. Holmes, J.N. Hacker, Climate change, thermal comfort and energy: Meeting the design challenges of the 21st century, Energy and Buildings, 39 (2007) 802-814.
21 A. Matzarakis, C. Endler, Climate change and thermal bioclimate in cities: impacts and options for adaptation in Freiburg, Germany, International Journal of Biometeorology, 54 (2010) 479-483.
22 R.L. Hwang, T.P. Lin, A. Matzarakis, Seasonal effects of urban street shading on long-term outdoor thermal comfort, Building and Environment, 46 (2011) 863-870.
23 A.M. Coutts, N.J. Tapper, J. Beringer, M. Loughnan, M. Demuzere, Watering our cities: The capacity for Water Sensitive Urban Design to support urban cooling and improve human thermal comfort in the Australian context, Progress in Physical Geography, 37 (2013) 2-28.
24 M.L. Lambert-Habib, J. Hidalgo, C. Fedele, A. Lemonsu, C. Bernard, How is climatic adaptation taken into account by legal tools? Introduction of water and vegetation by French town planning documents, Urban Climate, (2013).
25 A.R. Gentle, J.L.C. Aguilar, G.B. Smith, Optimized cool roofs: Integrating albedo and thermal emittance with R-value, Solar Energy Materials and Solar Cells, 95 (2011) 3207-3215.
26 J. Karlsson, L. Wadsö, M. Öberg, A conceptual model that simulates the influence of thermal inertia in building structures, Energy and Buildings, 60 (2013) 146-151.
27 H. Taha, D. Sailor, R. Ritschard, B. Huang, Database on albedo, surface moisture, and roughness length for meteorological simulations of the South Coast Air Basin, in: Lawrence Berkeley Laboratory Report No. 33051, 1992.
28 M. Santamouris, Environmental Design of Urban Buildings: An Integrated Approach, Taylor & Francis, 2012.
29 M.C. Baker, N.R.C.o. Canada, Roofs: design, application, and maintenance, Multiscience Publications, 1980.

30 S. Bretz, H. Akbari, A.H. Rosenfeld, H. Taha, Implementation of Solar Reflective Surfaces: Materials and Utility Programs, in: LBL Report 32467, University of California, Berkeley, 1992.
31 M. Roth, T.R. Oke, W.J. Emery, Satellite-derived urban heat islands from three coastal cities and the utilization of such data in urban climatology, International Journal of Remote Sensing, 10 (1989) 1699-1720.
32 J. Nichol, Remote sensing of urban heatislands by day and night, Photogrammetric Engineering and Remote Sensing, 71 (2005) 613-621.
33 L. Doulos, M. Santamouris, I. Livada, Passive cooling of outdoor urban spaces. The role of materials, Solar Energy, 77 (2004) 231-249.
34 B.-L. Wang, T. Takigawa, Y. Yamasaki, N. Sakano, D.-H. Wang, K. Ogino, Symptom definitions for SBS (sick building syndrome) in residential dwellings, International Journal of Hygiene and Environmental Health, 211 (2008) 114-120.
35 S.S.Y. Lau, F. Yang, Introducing Healing Gardens into a Compact University Campus: Design Natural Space to Create Healthy and Sustainable Campuses, Landscape Research, 34 (2009) 55-81.
36 T.-P. Lin, A. Matzarakis, R.-L. Hwang, Shading effect on long-term outdoor thermal comfort, Building and Environment, 45 (2010) 213-221.
37 F. Yang, S.S.Y. Lau, F. Qian, Thermal comfort effects of urban design strategies in high-rise urban environments in a sub-tropical climate, Architectural Science Review, 54 (2011) 285-304.
38 Y. Kikegawa, Y. Genchi, H. Kondo, K. Hanaki, Impacts of city-block-scale countermeasures against urban heat-island phenomena upon a building's energy-consumption for air-conditioning, Applied Energy, 83 (2006) 649-668.
39 M. Taleghani, D.J. Sailor, M. Tenpierik, A. van den Dobbelsteen, Thermal assessment of heat mitigation strategies: The case of Portland State University, Oregon, USA, Building and Environment, 73 (2014) 138-150.
40 R.A. Spronken-Smith, T.R. Oke, Scale Modelling of Nocturnal Cooling in Urban Parks, Boundary-Layer Meteorology, 93 (1999) 287-312.
41 C.R. Chang, M.H. Li, S.D. Chang, A preliminary study on the local cool-island intensity of Taipei city parks, Landscape and Urban Planning, 80 (2007) 386-395.
42 J.S. Reynolds, V. Carrasco, Shade water and mass: Passive cooling in Andalucia, in: National Passive Solar Conference, American Solar Energy Society, Boulder, CO, 1996.
43 T. Nakayama, T. Fujita, Cooling effect of water-holding pavements made of new materials on water and heat budgets in urban areas, Landscape and Urban Planning, 96 (2010) 57-67.
44 H. Radhi, F. Fikry, S. Sharples, Impacts of urbanisation on the thermal behaviour of new built up environments: A scoping study of the urban heat island in Bahrain, Landscape and Urban Planning, 113 (2013) 47-61.
45 M. Robitu, M. Musy, C. Inard, D. Groleau, Modeling the influence of vegetation and water pond on urban microclimate, Solar Energy, 80 (2006) 435-447.
46 T.R. Oke, J.M. Crowther, K.G. McNaughton, J.L. Monteith, B. Gardiner, The Micrometeorology of the Urban Forest [and Discussion], Philosophical Transactions of the Royal Society of London. B, Biological Sciences, 324 (1989) 335-349.
47 L. Howard, The climate of London, deduced from meteorological observations made in the metropolis and various places around it, Harvey and Darton, London, 1833.
48 A.H. Rosenfeld, H. Akbari, S. Bretz, B.L. Fishman, D.M. Kurn, D. Sailor, H. Taha, Mitigation of urban heat islands: materials, utility programs, updates, Energy and Buildings, 22 (1995) 255-265.
49 A. Dimoudi, M. Nikolopoulou, Vegetation in the urban environment: microclimatic analysis and benefits, Energy and Buildings, 35 (2003) 69-76.

50 C.S.B. Grimmond, M. Roth, T.R. Oke, Y.C. Au, M. Best, R. Betts, G. Carmichael, H. Cleugh, W. Dabberdt, R. Emmanuel, E. Freitas, K. Fortuniak, S. Hanna, P. Klein, L.S. Kalkstein, C.H. Liu, A. Nickson, D. Pearlmutter, D. Sailor, J. Voogt, Climate and More Sustainable Cities: Climate Information for Improved Planning and Management of Cities (Producers/Capabilities Perspective), Procedia Environmental Sciences, 1 (2010) 247-274.

51 E.G. McPherson, A.R. Rowntree, J.A. Wagar, Energy-efficient landscapes, in: G. Bradley (Ed.) Urban Forest Landscapes- Integrating Multidisciplinary Perspectives, University of Washington Press, Seattle/London, 1994.

52 T.R. Oke, The energetic basis of the urban heat island, Quarterly Journal of the Royal Meteorological Society, 108 (1982) 1-24.

53 H. Taha, S. Douglas, J. Haney, Mesoscale meteorological and air quality impacts of increased urban albedo and vegetation, Energy and Buildings, 25 (1997) 169-177.

54 L. Pereira, A. Perrier, R. Allen, I. Alves, Evapotranspiration: Concepts and Future Trends, Journal of Irrigation and Drainage Engineering, 125 (1999) 45-51.

55 D.J. Sailor, A review of methods for estimating anthropogenic heat and moisture emissions in the urban environment, International Journal of Climatology, 31 (2011) 189-199.

56 D.A. Montgomery, Landscaping as a passive solar strategy, Passive Solar Journal, 4 (1987) 79-108.

57 A. Moffat, M. Schiller, Landscape Design that Saves Energy, William Morrow and Company, New York, 1981.

58 H. Akbari, U.S.E.P.A.C.C. Division, L.B. Laboratory, U.S.D.o. Energy, Cooling our communities: a guidebook on tree planting and light-colored surfacing, U.S. Environmental Protection Agency, Office of Policy Analysis, Climate Change Division, 1992.

59 N.H. Wong, S.F. Tay, R. Wong, C.L. Ong, A. Sia, Life cycle cost analysis of rooftop gardens in Singapore, Building and Environment, 38 (2003) 499-509.

60 T. Carter, A. Keeler, Life-cycle cost–benefit analysis of extensive vegetated roof systems, Journal of Environmental Management, 87 (2008) 350-363.

61 FiBRE, Can greenery make commercial buildings more green? , in: Findings in Built and Rural Environments, Cambridge University, 2007.

62 G.B. Bonan, The microclimates of a suburban Colorado (USA) landscape and implications for planning and design, Landscape and Urban Planning, 49 (2000) 97-114.

63 L. Shashua-Bar, D. Pearlmutter, E. Erell, The cooling efficiency of urban landscape strategies in a hot dry climate, Landscape and Urban Planning, 92 (2009) 179-186.

64 J.H. Parker, Use of Landscaping for Energy Conversion, Department of Physical Sciences, Florida Internatioal University, Miami, FL, 1981.

65 A. Hoyano, Climatological uses of plants for solar control and the effects on the thermal environment of a building, Energy and Buildings, 11 (1988) 181-199.

66 O.B. Lay, L.G. Tiong, C. Yu, A survey of the thermal effect of plants on the vertical sides of tall buildings in Singapore, in: PLEA 2000, Cambridge, UK, 2000, pp. 495-500.

67 A.M. Papadopoulos, The influence of street canyons on the cooling loads of buildings and the performance of air conditioning systems, Energy and Buildings, 33 (2001) 601-607.

68 H.F. Castleton, V. Stovin, S.B.M. Beck, J.B. Davison, Green roofs; building energy savings and the potential for retrofit, Energy and Buildings, 42 (2010) 1582-1591.

69 I. Jaffal, S.-E. Ouldboukhitine, R. Belarbi, A comprehensive study of the impact of green roofs on building energy performance, Renewable Energy, 43 (2012) 157-164.

70 M. Santamouris, Environmental Design of Urban Buildings: An Integrated Approach, Taylor & Francis, 2013.

71 NEN-5060, Hygrothermische Eigenschappen van Gebouwen Referentieklimaatgegevens, in, Nederlands Normalisatie-Instituut (NNI), 2008.
72 M. Bruse, ENVI-met website, in, 2013.
73 M. Bruse, H. Fleer, Simulating surface–plant–air interactions inside urban environments with a three dimensional numerical model, Environmental Modelling & Software, 13 (1998) 373-384.
74 S. Huttner, M. Bruse, P. Dostal, Using ENVI-met to simulate the impact of global warming on the microclimate in central European cities in: H. Mayer, A. Matzarakis (Eds.) 5th Japanese-German Meeting on Urban Climatology, Meteorologischen Instituts der Albert-Ludwigs-Universität Freiburg, 2008, pp. 307-312.
75 M. Mahammadzadeh, Klimaschutz und Anpassung an die Klimafolgen: Strategien, Maßnahmen und Anwendungsbeispiele, IW-Medien, 2009.
76 N.H. Wong, S. Kardinal Jusuf, A. Aung La Win, H. Kyaw Thu, T. Syatia Negara, W. Xuchao, Environmental study of the impact of greenery in an institutional campus in the tropics, Building and Environment, 42 (2007) 2949-2970.
77 D. Taleb, B. Abu-Hijleh, Urban heat islands: Potential effect of organic and structured urban configurations on temperature variations in Dubai, UAE, Renewable Energy, 50 (2013) 747-762.
78 M. Kottek, J. Grieser, C. Beck, B. Rudolf, F. Rubel, World Map of the Köppen-Geiger climate classification updated, Meteorologische Zeitschrift, 15 (2006).
79 S. Wilcox, W. Marion, User's Manual for TMY3 Data Sets, NREL/TP-581-43156, in, Golden, Colorado: National Renewable Energy Laboratory, 2008.
80 KNMI, in: Climate Change Scenarios 2006 for the Netherlands, KNMI publication: WR-2006-01 2006.
81 M. Taleghani, M. Tenpierik, A. van den Dobbelsteen, Energy performance and thermal comfort of courtyard/atrium dwellings in the Netherlands in the light of climate change, Renewable Energy, 63 (2014) 486-497.
82 ISO7726, International Standard 7726, in: Ergonomics of the thermal environment - Instrument for measuring physical quantities, ISO Geneva, 1998.

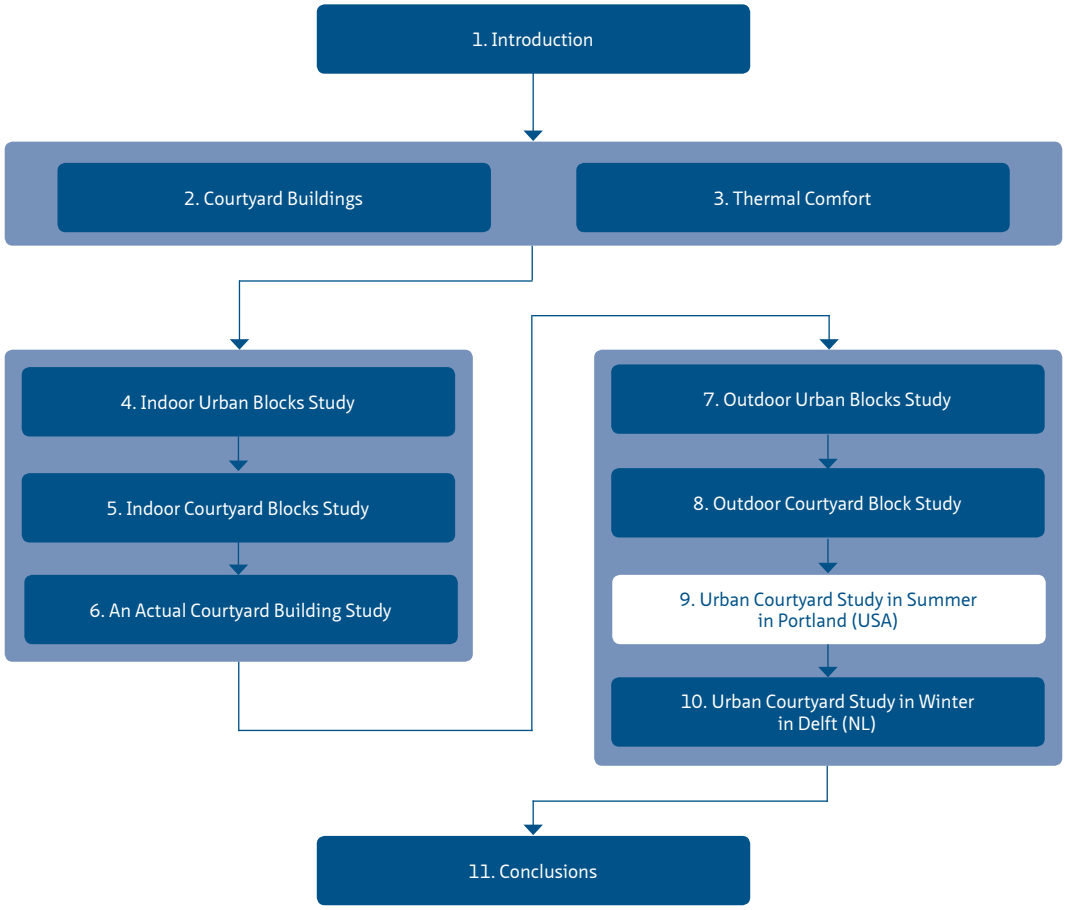
1. Introduction
2. Courtyard Buildings
3. Thermal Comfort
4. Indoor Urban Blocks Study
5. Indoor Courtyard Blocks Study
6. An Actual Courtyard Building Study
7. Outdoor Urban Blocks Study
8. Outdoor Courtyard Block Study
9. Urban Courtyard Study in Summer in Portland (USA)
10. Urban Courtyard Study in Winter in Delft (NL)
11. Conclusions